Bismuth vanadate photoanodes for water splitting deposited by radio-frequency plasma reactive co-sputtering

Running title: $BiVO_4$ photoanodes for water splitting

Running Authors: Pedroni et al.

Matteo Pedroni[1], Gian Luca Chiarello[2], Niloofar Haghshenas[2], Maurizio Canetti[3], Dario Ripamonti[4], Elena Selli[2] and Espedito Vassallo[1]

[1] CNR, Istituto di Fisica del Plasma "P. Caldirola", via R. Cozzi 53, 20125 Milano, Italy
[2] Dipartimento di Chimica, Università degli Studi di Milano, via C. Golgi 19, 20133 Milano, Italy
[3] CNR, Istituto per lo Studio delle Macromolecole, via E. Bassini 15, 20133 Milano, Italy
[4] CNR, Istituto di Chimica della Materia Condensata e di Tecnologie per l'energia, via R. Cozzi 53, 20125 Milano, Italy

[a)]Electronic mail: pedroni@ifp.cnr.it

Photoactive bismuth vanadate ($BiVO_4$) thin coatings were deposited on Fluorine-doped tin oxide (FTO) coated glass by plasma reactive sputtering from Bi_2O_3 and vanadium (V) radio-frequency (RF) powered targets. The films were characterized by XRD, SEM, EDS and UV-vis spectroscopy. The effects that the power density supplied to the Bi_2O_3 target, the post-annealing treatment and the film thickness have on the structural features and on the photoelectrochemical (PEC) performances of the so obtained $BiVO_4$ film-based photoelectrodes were investigated. Their PEC performance in water splitting was evaluated in a three-electrodes cell by both incident photon to current efficiency (IPCE) and linear sweep voltammetry measurements under AM 1.5G simulated solar light irradiation. A monoclinic phase of $BiVO_4$, which is more photoactive than the tetragonal $BiVO_4$ phase, was obtained by optimizing the power density supplied to the Bi_2O_3 target, i.e. by tuning the Bi:V:O atomic ratio. The best PEC performance was obtained for a stoichiometric 1:1 Bi:V atomic ratio, attained with 20 W power supplied at the Bi_2O_3 target and 300 W power supplied at the vanadium target, and an optimal 200 nm thickness of the $BiVO_4$ film, with a 0.65 mA/cm^2 photocurrent density attained at 1.23 V vs. SHE, under simulated solar light. These results show the

suitability of plasma reactive sputtering with two RF powered electrodes for the deposition of $BiVO_4$ photoanodes for water splitting.

I. INTRODUCTION

Photocatalysis with semiconductors has attracted considerable attention as an emerging promising technology for converting solar energy into chemical energy [1] and for the degradation of organic pollutants [2,3]. In particular, the photocatalytic water splitting process would provide hydrogen for fuel cell applications without consuming additional energy for its production. However, with most semiconductors, such as the widely employed TiO_2, the photocatalytic process can be activated only by UV light, which represents about 4% only of the incoming solar energy. This slowed down the commercialization of this technology up to now. Therefore, the development of innovative photocatalysts with visible-light-response, high efficiency and stability is still highly desirable for applications in the field of solar energy harvesting, conversion and storage.

Bismuth vanadate ($BiVO_4$) is one of the visible-light active semiconductor photocatalysts that is currently widely studied due to its steep absorption edge in the visible-light region [4,5]. The electronic and morphological materials properties are known to be crystal structure dependent and different crystalline forms can be synthesized by different preparation routes. Concerning $BiVO_4$ the most active phase under visible light irradiation appears to be the monoclinic scheelite one, with a band gap of 2.4 eV [6]. Furthermore, a variety of synthesis procedures has been used to obtain $BiVO_4$ films. The most frequently used techniques include wet chemistry combined with spin-coating [7], spray pyrolysis [8] and physical vapour deposition. In particular, the latter mainly refers to plasma sputtering processes by means of DC [9] or combined DC-RF powered electrodes [10,11].

In the present work, we investigate the deposition of visible light active $BiVO_4$ photolectrodes films by a plasma reactive sputtering process using two RF powered electrodes. This deposition method, being commercially available, highly scalable and widely applied in industry, might represent a feasible way to produce industrial scale photoelectrochemical (PEC) cell

applications. A systematic study has been performed on the effects that the elemental composition and the crystalline structure of the deposited material obtained under different deposition conditions have on the PEC activity of the photoelectrodes. Moreover, an investigation on the thickness of the $BiVO_4$ coating has been carried out in order to establish the optimum one.

II. EXPERIMENTAL

A. Deposition of $BiVO_4$ films

The $BiVO_4$ films were prepared by radio frequency (RF) plasma magnetron sputtering [12]. The reactor consists of a cylindrical stainless steel vacuum chamber equipped with two magnetron sputtering cathodes tilted at an angle of 20-30° with respect to a vertical axis. The cathodes are water cooled and connected to two separate RF (13.56 MHz) power supplies, coupled with an automatic impedance matching unit. The substrate holder, facing the targets, is grounded and rotating. Prior to film deposition, the reactor was evacuated to approximately 10−4 Pa. A co-sputtering approach was adopted, using separate bismuth oxide (Bi_2O_3, 99.9%) and metal vanadium (V, 99.99%) targets (Testbourne Ltd), both 3.0 inches in diameter. Because of their different thermal conductivity, two separated target power supplies were used in order to independently tune the Bi_2O_3 and V sputtering rates. The RF power of the metal vanadium target was fixed at 300 W (ca. 6 W/cm^2), while that of Bi_2O_3 was preliminarily investigated in the 15-30 W (0.33-0.66 W/cm^2) range.

The $BiVO_4$ films were deposited simultaneously on three different supports: i) 10 × 10 mm^2, 400 μm thick silicon wafers (for SEM, EDS and XRD analysis); ii) 15 × 60 mm^2, 0.50 mm thick Pyrex glass (for UV/Vis reflectance analysis), and iii) 10 × 40 mm^2, 2 mm thick fluorine doped tin oxide (FTO) conductive glass (for the photoelectrocatalytic tests). The supports were placed on the substrate holder rotated at a frequency of 1.5 rev/min and at a 10 cm distance from the targets. No bias voltage and heating were applied to the substrate holder. The deposition was performed in a

10% O_2/Ar reactive mixture at a constant pressure of 1.7 Pa. The deposition time was adjusted in order to reach a 100 nm film thickness.

A second series of photoelectrodes was prepared under the same conditions with a fixed 20 W power supplied at the Bi_2O_3 target and different deposition time (10-100 min), leading to a film thickness ranging from 50 nm to 500 nm.

All as deposited $BiVO_4$ films were amorphous; they were converted into crystalline $BiVO_4$ films by annealing in air at 400 °C for 2 h.

B. Characterization of $BiVO_4$ films

To evaluate the coating thickness, a portion of sample was covered with a silicon mask during the process. After that, taking it away, it was possible to measure the height difference between the deposited and non-deposited parts of the sample with a P15 surface profiler (KLA Tencor San Jose, CA). The structural properties were analyzed by X-ray diffraction (XRD) measurements, using a wide angle Siemens D-500 diffractometer equipped with a Siemens FK 60-10 2000 W tube. The phase identification was performed comparing the obtained patterns with the Inorganic Crystal Structure Database (ICSD).

The morphological and structural properties of the samples were investigated by scanning electron microscopy (SEM), using a high resolution SEM Hitachi SU70 instrument with Schottky electron source and secondary electron (SE) in-column upper-detector. Standard elemental analysis through energy dispersion spectroscopy (EDS) was obtained with the NORAN 7, Thermo Scientific EDS system. Moreover cross section images were used to check the films thickness measured by the profilometer.

UV-Vis-NIR diffuse reflectance spectra were recorded in the 220-2600 nm range with a Shimadzu UV3600 Plus spectrophotometer equipped with an ISR-603 integrating sphere. Barium sulfate was used as the reference standard.

C. Photocatalytic water splitting tests

Incident photon to current efficiency (IPCE) and linear sweep voltammetry (LSV) tests under simulated AM 1.5G solar light (300 W LOT-qd Xe lamp, equipped with an AM 1.5G filter) were performed using a three-electrode homemade photoelectrocatalytic (PEC) cell, with the $BiVO_4$ film deposited on FTO being the working electrode, a Pt wire the counter electrode and a standard calomel electrode (SCE) the reference electrode. They were all connected to an Amel, mod. 2549 potentiostat/galvanostat and immersed in a 0.5 M Na_2SO_4 electrolyte solution at pH 7. All measurements were performed under N_2 bubbling into the electrolyte solution; N_2 bubbling always started 20 min prior to the beginning of the tests.

In the simulated solar light tests, the photoelectrode was placed at ca. 50 cm from the light source in order to have an incident power of 100 mW cm^{-2} on the photoactive surface. IPCE measurements were performed with the 300 W Xe lamp connected to a LOT-qd Omni-λ 150 monochromator. The incident power was measured with a calibrated Thorlabs S130VC photodiode connected to a Thorlabs PM200 power meter. Measurements were done at 1 V vs. SCE. The percent IPCE at each wavelength λ was calculated as:

$$\%\, IPCE = \frac{i_\lambda}{P_\lambda} \cdot \frac{1240}{\lambda} \cdot 100, \quad (1)$$

where iλ is the photocurrent density (mA cm^{-2}) at a specific incident λ (nm), Pλ is the incident power density (mW cm^{-2}) at the same λ, and 1240 (in J nm C^{-1}) is h c q^{-1}, h being the Planck constant, c the speed of light and q the charge of a single electron.

III. RESULTS AND DISCUSSION

A. Photoanodes characterization

In this work, we report the development of a reactive co-sputtering procedure using separate bismuth oxide and vanadium metal targets powered by RF to produce $BiVO_4$ thin films. The series of thin films, deposited at a fixed 300 W power to the V target and at different power (from 15 to 30 W) supplied to the Bi_2O_3 target, after annealing showed colors varying from orange to yellow (see

Fig. 1), the film prepared at 15 W being orange and all the others (prepared at 20 to 30 W) showing different shadows of yellow.

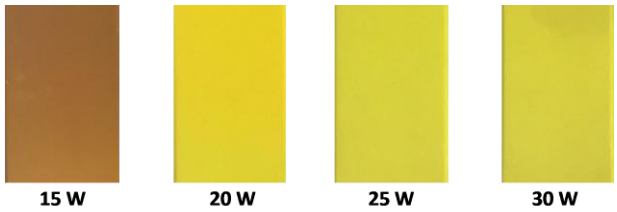

FIG. 1. Films deposited on Pyrex glass obtained at different power supplied to the Bi_2O_3 target.

The X-ray diffraction (XRD) patterns obtained from these films match well those of the monoclinic BiVO4 phase [13-16], with the characteristic peaks of this latter located at 2θ 18.7° (011), 28.8° (121), 30.5° (040), 40.0° (211), 46.7° (240), 47.3° (042), 53.4° (161) and 58.5° (321).

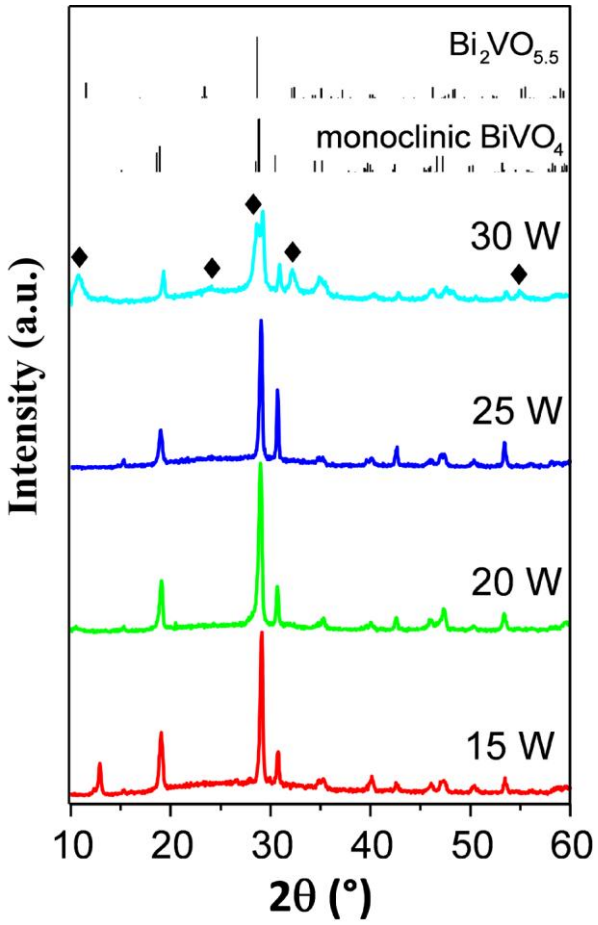

FIG. 2. X-ray diffraction patterns of $BiVO_4$ coatings deposited at different power supplied at the Bi_2O_3 target. The peak positions and relative intensities of the monoclinic $BiVO_4$ (ICSD code 100604) and $Bi2VO_{5.5}$ (ICSD code 85181) phases are reported on top for comparison. The peaks of the latter are indicated with ♦ on the top pattern.

As shown in Fig. 2, the sample deposited at 30 W (Bi rich sample) clearly shows some extra peaks at 2θ 11.3° (020), 23.9° (111), 28.6° (131), 32.2° (200), 48.3 (260) and 54.8° (262), which have been attributed to the $Bi_2VO_{5.5}$ phase. No characteristic peaks of BiO_x or VO_x phases can be observed. However, only the pattern of the sample deposited at 20 W (stoichiometric Bi:V ratio of 1:1) shows a flat baseline, whereas all the other samples displace a broad hump in the baseline, very likely due to the presence of amorphous components of BiO_x and/or VO_x.

The deposition rate of the films, estimated by dividing the film thickness by the deposition time, increased with increasing power supplied to the Bi_2O_3 target and were found to be 4.2, 4.6, 5.9 and 7.3 nm/min, for 15, 20, 25 and 30 W supplied powers, respectively. Moreover, the morphology of the sputtered thin coatings, determined through scanning electron microscope (SEM) images, did not change in the considered range of power supplied to the Bi_2O_3 target. Fig. 3 exemplarily shows the SEM images of the film deposited at 20 W, evidencing a dense and uniform coating with a relatively smooth surface and a hundred of nanometers grain size.

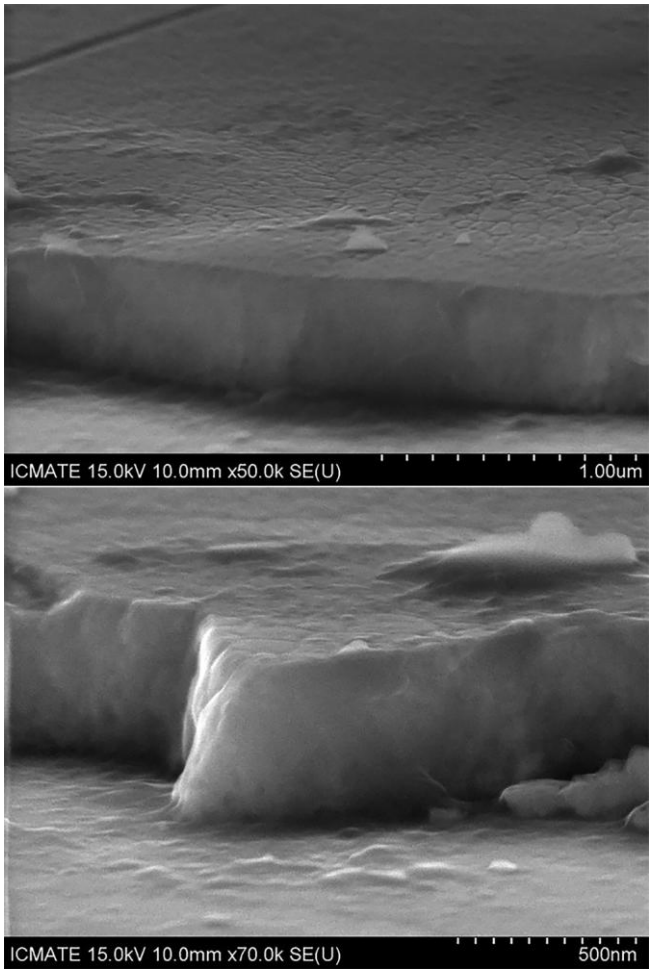

FIG. 3. SEM images at two different magnifications of the $BiVO_4$ film deposited at 20 W power supplied at the Bi_2O_3 target.

Energy Dispersion Spectroscopy (EDS) was used to evaluate the elemental composition of the deposited samples. The EDS spectra confirm the presence of Bi, V and O elements. The EDS data obtained with films deposited at different power (from 15 to 30 W) supplied to the Bi_2O_3 target are reported in Table 1. The percent amount of bismuth increases with increasing power supplied to the Bi_2O_3 target; the coating deposited at 20 W exhibits an optimal Bi:V stoichiometric ratio, as demonstrated by the atomic percent amounts of bismuth, vanadium and oxygen (1:1:~4).

TABLE I. Elemental composition (atom %) of four films deposited at different power supplied at the Bi_2O_3 target.

Power / W	O / at%	V / at%	Bi / at%	V/Bi	O/Bi
15	70	19.3	10.7	1.8	6.6
20	66.3	16.7	16.9	1.0	3.9
25	65.8	14.9	19.1	0.8	3.4
30	65.6	13	21	0.6	3.1

The UV-Vis diffuse reflectance spectra (DRS) reported in Fig. 4 provide information on the optical properties and the electronic states in semiconductor materials [17]. All deposited films exhibit a steep absorption edge in the visible region ascribable to the band gap transition [18] and a strong absorption in the visible range (450-700 nm).

The band gap energy of samples can be calculated by eq. 2:

$\alpha h\nu = A\ (h\nu - Eg)n$, (2)

where α is the absorption coefficient of the material, ν is the frequency of light, A is a constant, Eg is the band gap energy [19], and n is a coefficient which depends on the characteristics of the semiconductor transition. In the present case, the value of n is 2, for indirect allowed transitions [20,21]. The diffuse reflectance data were used to calculate the absorption coefficient α from the $F(R\infty)$ Kubelka–Munk (KM) function [22]. The optical energy gap Eg of the investigated thin films can be evaluated by plotting the data obtained from DRS analysis in terms of $(F(R\infty)E)^{1/2}$ versus the photon energy ($h\nu$) and by drawing a line tangent to the plotted curve, as shown in Fig. 4. The point of intersection of this line with the abscissa axis provides an estimated value of the band gap energy.

The band gap of the film prepared at 15 W supplied bias (orange color) was found to be 2.05 eV, while for films obtained by deposition with 20-30 W supplied power (yellow colors) the band gap was found to increase from 2.46 to 2.57 eV with increasing Bi_2O_3 target power density

(i.e. with increasing the Bi/V ratio, see Table 1). Such band gap values are in good agreement with those reported in the literature for $BiVO_4$ [23-25].

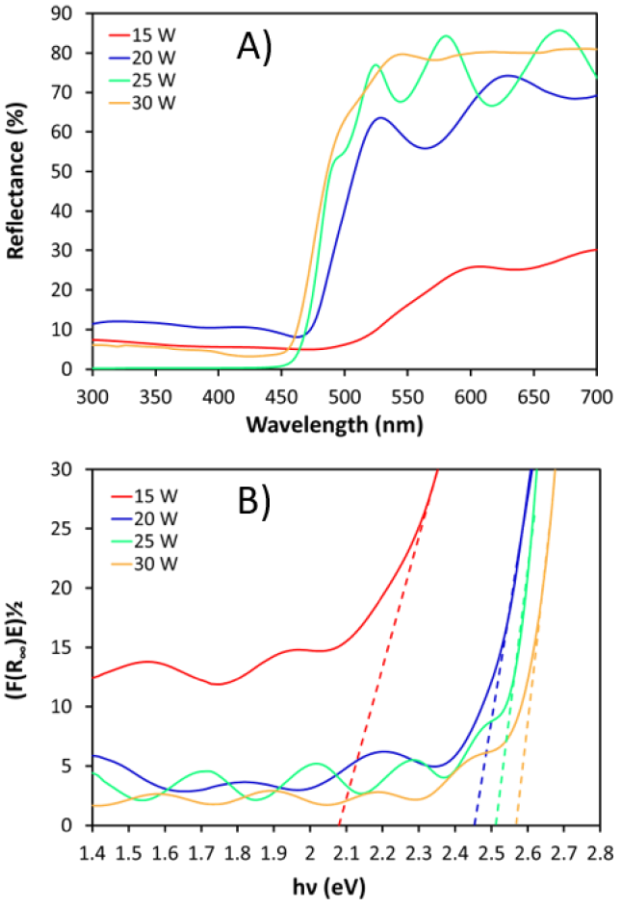

FIG. 4. Diffuse reflectance spectra (DRS) of $BiVO_4$ films deposited at different power supplied at the Bi_2O_3 target (A) and Tauc plot for the estimation of their optical absorption edge energy (B).

B. Effect of the power at the Bi_2O_3 target on the photoelectrocatalytic activity

The PEC performance of the $BiVO_4$ films was evaluated by employing them as photoanodes in the water splitting reaction. Fig. 5 shows the chopped J-V curves acquired with the photoelectrodes under front and back (i.e. through the FTO support) illumination, where the current density is a function of the applied potential in the PEC system.

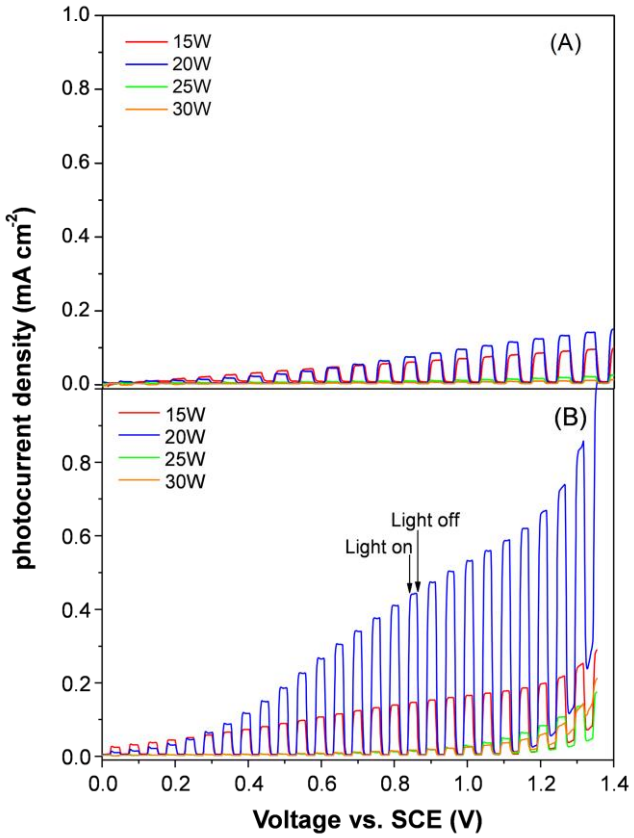

FIG. 5. Effect of the Bi_2O_3 target power on the chopped J−V (current density vs. voltage) curves of the $BiVO_4$ films under (A) front and (B) back AM 1.5G illumination in 0.5 M Na_2SO_4 electrolyte solution at pH 7.

The highest photocurrent density was attained with the film deposited at 20 W, having the right 1:1:~4 Bi:V:O stoichiometric ratio of $BiVO_4$ (Table 1). Fig. 5 also shows a significant difference of the photocurrent density recorded under front and back illumination. The superior PEC performance of $BiVO_4$ coatings when illuminated from the back (FTO side) rather than form the front ($BiVO_4$ side) has already been reported [26] and attributed to the poor electron mobility in bulk $BiVO_4$ [10]. Indeed, when the electron-hole couples are produced in a $BiVO_4$ region opposite to that in contact with the FTO conducting glass the photogenerated charge carriers must travel across the entire film thickness to reach it. Therefore, due to the electron mobility limitations, the electron-hole recombination probability is relatively high, which leads to a low photocurrent. Under back illumination this effect is mitigated because of the minimized transport length from the photoexcitation region to the FTO conducting glass.

Fig. 6 displays the IPCE of the $BiVO_4$ photoanodes. The photoanode deposited at 20 W clearly is the best performing one, with an activity onset at wavelength longer than 500 nm in agreement with the Eg value calculated from DRS analysis. On the contrary, the coating deposited at 15 W showed only a very low activity in the 450-500 nm range and a higher activity below 410 nm. Thus, the superior performance of the photoanode deposited at 20 W results from both its higher IPCE response and its ability to harvest and convert a larger portion of solar light.

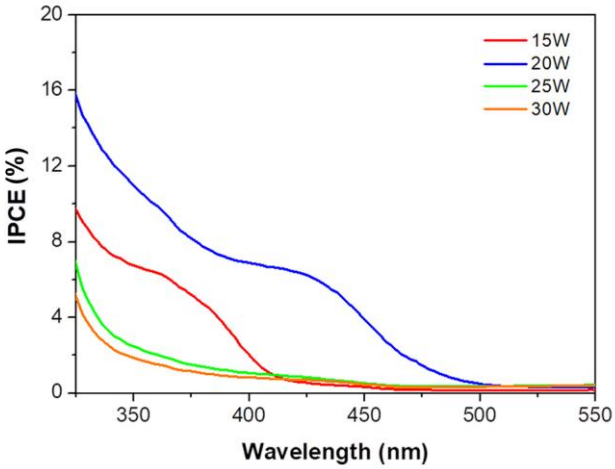

FIG. 6. Incident photon to current efficiency (IPCE) curves of the investigated photoanodes under back irradiation at 1.0 V vs. SCE in a 0.5 M Na_2SO_4 electrolyte solution.

C. Effect of the $BiVO_4$ film thickness on the photoelectrocatalytic activity

The film deposited at 20 W thus exhibits the highest PEC performance. Hence, a second series of $BiVO_4$ films were deposited on FTO at a fixed 20 W power of the Bi_2O_3 target with different deposition time in order to study the effect of the film thickness (ranging from 50 nm to 500 nm) on the photocurrent density. The results are shown in Fig. 7.

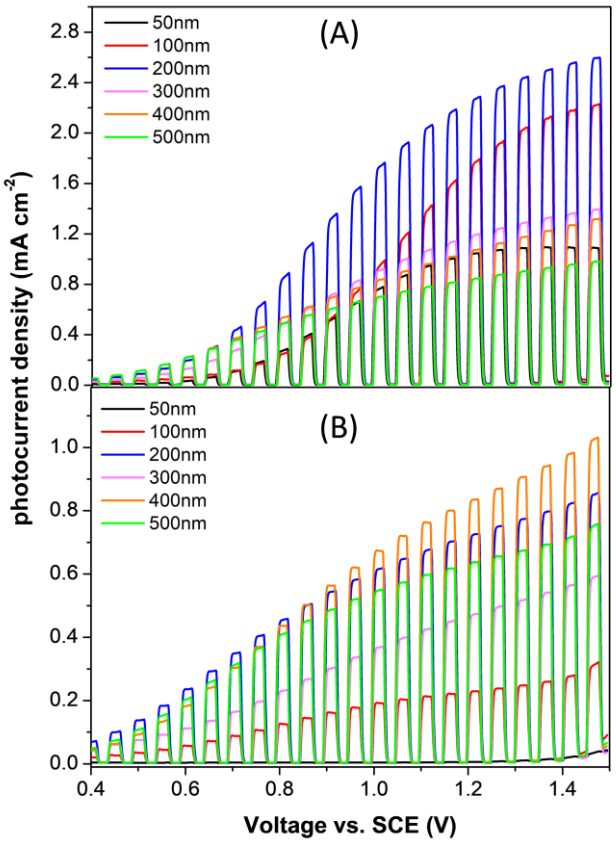

FIG. 7. Influence of the $BiVO_4$ film thickness in photoanodes on the chopped J−V (current density vs. voltage) curves under back AM 1.5G illumination in 0.5 M Na_2SO_4 electrolyte solution at pH 7: (A) as prepared photoelectrodes, (B) aged photoelectrodes.

The photoanodes exhibited an exceptionally high photocurrent density (Fig. 7A), up to 2.8 mA cm^{-2} at 1.4 V vs. SCE in the case of the 200 nm thick film. However, such a high photocurrent considerably dropped down during the subsequent chronoamperometric stability tests (see Fig. 8) at 1.0 V vs. SCE under 90 min-long solar light illumination (3 cycles of 30 min each). Fig. 8 shows that the thinner films (50, 100 and 200 nm thick) underwent a pronounced photocurrent drop, while the thickest 500 nm thick film exhibited the highest stability. A thicker film could protect the FTO-$BiVO_4$ junction from the contact with the electrolyte solution, thus preventing its possible dissolution and finally ensuring a better electrical contact along the time. In fact, it is well known that $BiVO_4$ suffers of low chemical stability [27] because it can gradually dissolves in strong basic and acidic solutions. In order to slow down its dissolution the tests were performed at pH 7.

With all photoelectrodes a photocurrent peak was observed as the light was switched on, likely due to a hole accumulation due to a hole diffusion slower than photopromoted electron diffusion.

The linear sweep voltammetry under chopped simulated solar light (back illumination) performed with the same photoanodes after the stability tests (see Fig. 7B) shows a significantly lower photocurrent density of the thinner films (50, 100 and 200 nm thick), while that of thickest film remained almost the same. The highest photocurrent of ca. 1 mA cm^{-2} was reached by the 400 nm thick sample at 1.4 V vs. SCE. The effects of both film thickness and irradiation mode (front or back) can be appreciated in Fig. 9.

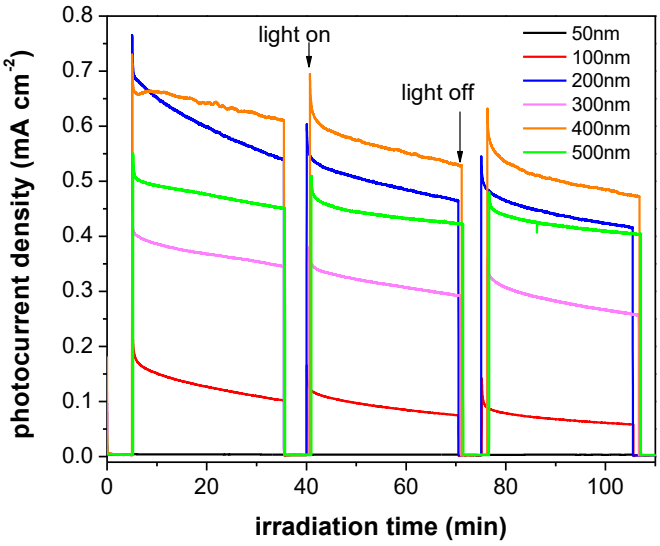

FIG. 8. Time stability of the series of photoanodes with a film thickness ranging from 50 nm to 500 nm at 1.0 V vs. SCE under back AM 1.5G illumination in a 0.5 M Na_2SO_4 electrolyte solution.

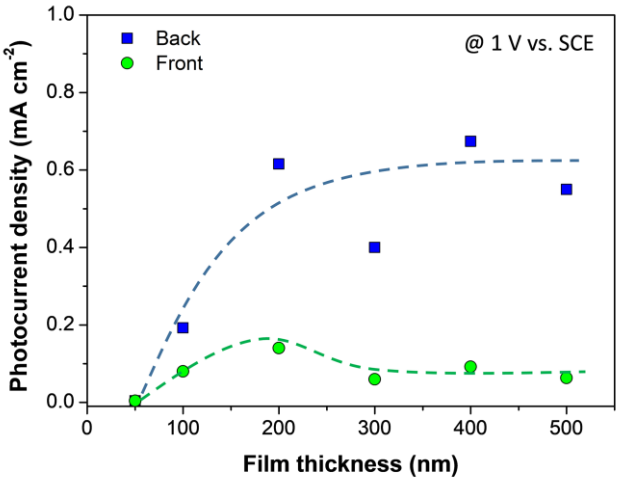

FIG. 9. Effect of the film thickness on the photocurrent density at 1.0 V vs. SCE under (●) front or (■) back AM 1.5G illumination in 0.5 M Na_2SO_4 electrolyte solution.

The photocurrent density obtained under back illumination (jFTO) is always higher than that obtained under front illumination ($jBiVO_4$). Moreover, the front and back illumination follow a different trend as a function of the film thickness, though both increasing with an increase of the film thickness up to ca. 200 nm. Indeed, the thicker the coating, the larger the amount of absorbed photons leading to a higher current density. For a thickness above 200 nm, $jBiVO_4$ decreases with an increase of the thickness, while jFTO reaches a sort of plateau at about 0.65 mA cm^{-2}.

The main difference between the front and the back illumination consists in the length of the diffusion path of photopromoted electrons from the site where charge carriers are generated to the $BiVO_4$/FTO interface where the electrons are transferred to the Pt counter electrode through the external circuit. In the case of front illumination, a decrease of photocurrent density is expected when the film thickness is wider than the mean electron diffusion path, i.e. the mean distance that the electrons can travel within the $BiVO_4$ film before recombining with a hole. Thus, the probability of charge carrier recombination increases with an increase of the electron diffusion path towards the FTO glass leading to the lower photocurrent observed for a film thickness above 200 nm. In contrast, in the case of back irradiation the majority of photons are absorbed close to the $BiVO_4$/FTO interface. Thus, when the film thickness exceeds the mean diffusion path, the photocurrent density reaches a plateau because the electrons eventually photopromoted at a distance from the FTO glass exceeding their mean diffusion path are lost due to recombination. Hence, our results suggest that the mean electron diffusion path within our $BiVO_4$ film is ca. 200 nm.

IV. Conclusions

Reactive RF co-magnetron sputtering from Bi_2O_3 and V targets was successfully employed to deposit photoactive $BiVO_4$ films on FTO. A coating composed, after annealing, mainly of monoclinic scheelite phase with the correct Bi/V stoichiometric ratio was obtained by optimizing the power density supplied to the Bi_2O_3 target. The PEC activity of the so obtained photoanodes

was investigated in a home-made 3 electrodes and single compartment PEC cell. The best performing photoanode being the one obtained with the 1:1 Bi:V ratio (average photocurrent density of 0.65 mA/cm^2 at 1.23 V). Experiments performed with 50 to 500 nm thick films confirm that under back illumination the charge diffusion is more efficient than that under front illumination, and that the photocurrent density is clearly thickness dependent, the optimal thickness being around 200 nm.

Acknowledgement

This work was supported within the CNR-Regione Lombardia agreement n° 19366/RCC, January 10th 2017. Decr. Reg. n.7784 - 05/08/2016 and the MIUR PRIN 2015K7FZLH project entitled Solar driven chemistry: new materials for photo- and electro-catalysis.

References

[1] F. E. Osterloh, ACS Energy Lett. **2**, 445 (2017).

[2] Z. Miao, G. Wang, L. Li, C. Wang, and X. Zhang, J. Mater. Sci. **54**, 14320 (2019).

[3] X. Dang, X. Zhang, W. Zhang, X. Dong, G. Wang, C. Ma, X. Zhang, H. Ma and M. Xue, RSC Adv. **5**, 15052 (2015).

[4] Q. Jia, K. Iwashina, and A. Kudo, PNAS **109,** 11564 (2012).

[5] X. Zhang, L. Du, H. Wang, X. Dong, X. Zhang, C. Ma, and H. Ma, Micropor. Mesopor. Mater. **173**, 175 (2013).

[6] A. Kubacka, M. Fernández-García, and G. Colón, Chem. Rev. **112**, 1555 (2012).

[7] I. Grigioni, A. Corti, M. V. Dozzi, and E. Selli, J. Phys. Chem. C **122**, 13969 (2018).

[8] F.F. Abdi, N. Firet, and R.v. de Krol, ChemCatChem. **5**, 490 (2013).

[9] H. Gong, N. Freudenberg, M. Nie, R. van de Krol, and K. Ellmer, AIP. Adv. **6**, 045108 (2016).

[10] L. Chen, E.A. Lladó, M. Hettick, I.D. Sharp, Y. Lin, A. Javey, and J.W. Ager, J. Phys. Chem. C **117**, 21635 (2013).

[11] S. M. Thalluri, R. M. Rojas, O. D. Rivera, S. Hernàndez, N. Russo, and S. E. Rodil, Phys. Chem. Chem. Phys. **17**, 17821 (2015).

[12] P.J. Kelly, and R.D. Arnell, Vacuum **56**, 159 (2000).

[13] S. Kunduz, and G.S.P. Soylu, Sep. Purif. Technol. **141,** 221 (2015).

[14] S.S. Fathimah, P.P. Rao, V. James, A.K.V. Raj, and G.R. Chitradevi, Dalton T. **43**, 15851 (2014).

[15] Y. Shen, M. Huang, Y. Huang, J. Lin, and J. Wu, J. Alloy. Compd. **496**, 287 (2010).

[16] M. Shang, W. Wang, L. Zhou, S. Sun, and W. Yin, J. Hazard. Mater. **172**, 338 (2009).

[17] J.Q. Yu, and A. Kudo, Adv. Funct. Mater. **16**, 2163 (2006).

[18] L. Zhou, W.Z. Wang, L.S. Zhang, H.L. Xu, and W. Zhu, J. Phys. Chem. C **111,** 13659 (2007).

[19] N.F. Mott, and E.A. Davis, Electronic Processes in Non-crystalline Materials, Clarendon Press, Oxford, 1979.

[20] A.S. Hassanien, and A.A. Akl, Superlattice. Microst. **89**, 153 (2016).

[21] J.K. Cooper, S. Gul, F.M. Toma, L. Chen, Y.S. Liu, J. Guo, J. W. Ager, J. Yano, and I.D. Sharp, J. Phys. Chem. C **119**, 2969 (2015).

[22] P. Kubelka, and F. Munk, An Article on Optics of Paint Layers, Z. Tech. Phys. **12**, 593 (1931).

[23] S. Tokunaga, H. Kato, and A. Kudo, Chem. Mater. **13** 4628 (2001).

[24] Y. Zhou, K. Vuille, A. Heel, B. Probst, R. Kontic, and G.R. Patzke, Appl. Catal. A-Gen. **375**, 140 (2010).

[25] T. Jafari, E. Moharreri, A.S. Amin, R. Miao, W. Song, and S. L. Suib, Molecules **21**, 900 (2016).

[26] W. Luo, Z. Yang, Z. Li, J. Zhang, J. Liu, Z. Zhao, Z. Wang, S. Yan, T. Yu, and Z. Zou, Energ. Environ. Sci. **4**, 4046 (2011).

[27] T. W. Kim, and K.-S. Choi, J. Phys. Chem. Lett. **7**, 447, (2016).